Er-fiber laser enabled, energy scalable femtosecond source tunable from 1.3 to 1.7 μm

HSIANG-YU CHUNG,[1,2] WEI LIU,[1,2] QIAN CAO,[1,2] FRANZ X. KÄRTNER,[1,2,3] AND GUOQING CHANG[1,3,*]

[1]*Center for Free-Electron Laser Science, DESY, Notkestraße 85, 22607 Hamburg, Germany*
[2]*Physics Department, University of Hamburg, Luruper Chaussee 149, 22761 Hamburg, Germany*
[3]*The Hamburg Centre for Ultrafast Imaging, Luruper Chaussee 149, 22761 Hamburg, Germany*
**guoqing.chang@desy.de*

Abstract: We demonstrate that energetic femtosecond pulses tunable from 1.3 to 1.7 μm can be achieved using self-phase modulation enabled spectral broadening followed by spectral lobe filtering. Based on a home-built 5-W Er-fiber laser system operating at 31-MHz repetition rate, we obtain femtosecond pulses that can be continuously tuned from 1.3 to 1.7 μm with >4.5 nJ pulse energy. We further optimize the spectral broadening process using a fiber with larger mode area and scale up the pulse energy to >10 nJ; the resulting pulse duration is as short as ~50 fs. Such a widely tunable, energetic femtosecond source is well suited for driving a laser scanning microscope to perform deep tissue multiphoton microscopy.

OCIS codes: (060.7140) Ultrafast processes in fibers; (060.4370) Nonlinear optics, fibers.

References and links

1. W. R. Zipfel, R. M. Williams, and W. W. Webb, "Nonlinear magic: multiphoton microscopy in the biosciences," Nat. Biotechnol. **21**(11), 1369–1377 (2003).
2. K. Svoboda and R. Yasuda, "Principles of two-photon excitation microscopy and its applications to neuroscience," Neuron **50**(6), 823–839 (2006).
3. E. E. Hoover and J. A. Squier, "Advances in multiphoton microscopy technology," Nat. Photonics **7**(2), 93–101 (2013).
4. T. Gottschall, T. Meyer, M. Schmitt, J. Popp, J. Limpert, and A. Tünnermann, "Four-wave-mixing-based optical parametric oscillator delivering energetic, tunable, chirped femtosecond pulses for non-linear biomedical applications," Opt. Express **23**(18), 23968–23977 (2015).
5. J. P. Epping, M. Kues, P. J. M. van der Slot, C. J. Lee, C. Fallnich, and K. J. Boller, "Integrated CARS source based on seeded four-wave mixing in silicon nitride," Opt. Express **21**(26), 32123–32129 (2013).
6. M. Brinkmann, S. Dobner, and C. Fallnich, "Light source for narrow and broadband coherent Raman scattering microspectroscopy," Opt. Lett. **40**(23), 5447–5450 (2015).
7. H.-W. Chen, Z. Haider, J. Lim, S. Xu, Z. Yang, F. X. Kärtner, and G. Chang, "3 GHz, Yb-fiber laser-based, few-cycle ultrafast source at the Ti:sapphire laser wavelength," Opt. Lett. **38**(22), 4927–4930 (2013).
8. M.-C. Chan, C.-H. Lien, J.-Y. Lu, and B.-H. Lyu, "High power NIR fiber-optic femtosecond Cherenkov radiation and its application on nonlinear light microscopy," Opt. Express **22**(8), 9498–9507 (2014).
9. F. Tauser, F. Adler, and A. Leitenstorfer, "Widely tunable sub-30-fs pulses from a compact erbium-doped fiber source," Opt. Lett. **29**(5), 516–518 (2004).
10. H. Tu, J. Lægsgaard, R. Zhang, S. Tong, Y. Liu, and S. A. Boppart, "Bright broadband coherent fiber sources emitting strongly blue-shifted resonant dispersive wave pulses," Opt. Express **21**(20), 23188–23196 (2013).
11. H. Lim, J. Buckley, A. Chong, and F. W. Wise, "Fibre-based source of femtosecond pulses tunable from 1.0 to 1.3 microns," Electron. Lett. **40**(24), 1523–1525 (2004).
12. J. Takayanagi, T. Sugiura, M. Yoshida, and N. Nishizawa, "1.0-1.7-um wavelength tunable ultrashort-pulse generation using femtosecond Yb-doped fiber laser and photonic crystal fiber," IEEE Photonics Technol. Lett. **18**(21), 2284–2286 (2006).
13. M.-C. Chan, S.-H. Chia, T.-M. Liu, T.-H. Tsai, M.-C. Ho, A. A. Ivanov, A. M. Zheltikov, J.-Y. Liu, H.-L. Liu, and C.-K. Sun, "1.2-2.2-um tunable Raman soliton source based on a Cr:Forsterite-laser and a Photonic-Crystal Fiber," IEEE Photonics Technol. Lett. **20**(11), 900–902 (2008).
14. J. Lim, H.-W. Chen, S. Xu, Z. Yang, G. Chang, and F. X. Kärtner, "3 GHz, watt-level femtosecond Raman soliton source," Opt. Lett. **39**(7), 2060–2063 (2014).

15. K. Wang and C. Xu, "Tunable high-energy soliton pulse generation from a large-mode-area fiber and its application to third harmonic generation microscopy," Appl. Phys. Lett. **99**(7), 071112 (2011).
16. H. Kawagoe, S. Ishida, M. Aramaki, Y. Sakakibara, E. Omoda, H. Kataura, and N. Nishizawa, "Development of a high power supercontinuum source in the 1.7 μm wavelength region for highly penetrative ultrahigh-resolution optical coherence tomography," Biomed. Opt. Express **5**(3), 932–943 (2014).
17. P. Cadroas, L. Kotov, L. Abdeladim, M. Likhachev, D. Lipatov, A. Hideur, W. Supatto, J. Livet, E. Beaurepaire, and S. Février, "Three-photon microscopy with a monolithic all-fiber format laser emitting at 1650 nm," in *Advanced Photonics Congress 2016 (IPR, NOMA, Sensors, Networks, SPPCom, SOF),* OSA Technical Digest (online) (Optical Society of America, 2016), paper SoM4F.4.
18. J. W. Nicholson, A. Desantolo, W. Kaenders, and A. Zach, "Self-frequency-shifted solitons in a polarization-maintaining, very-large-mode area, Er-doped fiber amplifier," Opt. Express **24**(20), 23396–23402 (2016).
19. N. G. Horton, K. Wang, D. Kobat, C. G. Clark, F. W. Wise, C. B. Schaffer, and C. Xu, "*In vivo* three-photon microscopy of subcortical structures within an intact mouse brain," Nat. Photonics **7**(3), 205–209 (2013).
20. K. Wang, N. G. Horton, and K. Charan, "Advanced fiber soliton sources for nonlinear deep tissue imaging in biophotonics," IEEE J. Sel. Top. Quantum Electron. **20**(2), 6800311 (2014).
21. W. Liu, C. Li, Z. Zhang, F. X. Kärtner, and G. Chang, "Self-phase modulation enabled, wavelength-tunable ultrafast fiber laser sources: an energy scalable approach," Opt. Express **24**(14), 15328–15340 (2016).
22. W. Liu, S.-H. Chia, H.-Y. Chung, R. Greinert, F. X. Kärtner, and G. Chang, "Energetic ultrafast fiber laser sources tunable in 1030-1215 nm for deep tissue multi-photon microscopy," Opt. Express **25**(6), 6822–6831 (2017).
23. S. W. Hell, K. Bahlmann, M. Schrader, A. Soini, H. M. Malak, I. Gryczynski, and J. R. Lakowicz, "Three-photon excitation in fluorescence microscopy," J. Biomed. Opt. **1**(1), 71–74 (1996).
24. D. G. Ouzounov, T. Wang, M. Wang, D. D. Feng, N. G. Horton, J. C. Cruz-Hernández, Y.-T. Cheng, J. Reimer, A. S. Tolias, N. Nishimura, and C. Xu, "*In vivo* three-photon imaging of activity of GCaMP6-labeled neurons deep in intact mouse brain," Nat. Methods **14**(4), 388–390 (2017).
25. D. Fehrenbacher, P. Sulzer, A. Liehl, T. Kälberer, C. Riek, D. V. Seletskiy, and A. Leitenstorfer, "Free-running performance and full control of a passively phase-stable Er:fiber frequency comb," Optica **2**(10), 917–923 (2016).
26. C. Xu, W. Zipfel, J. B. Shear, R. M. Williams, and W. W. Webb, "Multiphoton fluorescence excitation: new spectral windows for biological nonlinear microscopy," Proc. Natl. Acad. Sci. U.S.A. **93**(20), 10763–10768 (1996).

1. Introduction

Ultrafast sources emitting femtosecond pulses with the center wavelength continuously tunable are desired in many microscopy and spectroscopy applications. For example, broad deployment of two-photon excitation fluorescence microscopy has stimulated intense research efforts in developing femtosecond sources in the 800-1300 nm wavelength range, because most of the commonly used fluorophores have their two-photon excitation wavelength in this range [1–3]. Tunable femtosecond sources normally consist of a source laser producing femtosecond pulses at a certain wavelength and a nonlinear optical device converting them to wavelength tunable femtosecond pulses. An exemplary combination is a mode-locked laser plus a synchronously pumped solid-state optical parametric oscillator (OPO). Different from solid-state OPOs that rely on the second-order nonlinearity in optical crystals, the third-order nonlinearity associated with optical fibers offers an alternative means of generating widely tunable femtosecond pulses. Several fiber-optic nonlinear mechanisms—such as four-wave mixing [4–6], dispersive wave generation [7–10], soliton self-frequency shift (SSFS) [9,11–20] etc.—can significantly expand the wavelength coverage of an input narrowband spectrum. However four-wave mixing method normally results in sub-picosecond or picosecond pulses. For example, Ref. 4 uses a μJ-level fiber laser system at 1040 nm to drive a fiber OPO enabled by four-wave mixing and produces 560-fs pulses after post compression with 30-nJ pulse energy. Dispersive wave generation can generate pulses below 100 fs. However, the wavelength tunability is limited to ~100 nm due to the phase matching requirement between the dispersive wave and the soltion that emits it. SSFS continuously red-shifts the center wavelength of a femtosecond pulse propagating inside an optical fiber with negative group-velocity dispersion (GVD). The amount of wavelength shift can be tuned by varying the input pulse energy. Use of large more-area (LMA) fibers can increase the pulse energy. For example, SSFS in a photonic crystal rod with a mode area of 2300 μm^2 can generate 67-nJ pulses at 1675 nm [19,20]. Unfortunately SSFS

can only lead to the tunable pulses with the center wavelength longer than the pump wavelength. This implies that use of Er-fiber laser as the pump can only generate tunable pulse beyong 1550 nm.

Recently, we demonstrated a new fiber-optic method of generating widely wavelength tunable femtosecond pulses [21]. The method employs self-phase modulation (SPM) dominated nonlinearities to broaden an input optical spectrum, followed by optical bandpass filters to select the leftmost or rightmost spectral lobes. Unlike SSFS that always red-shifts an input spectrum, SPM-enabled spectral broadening can generate both blue-shifted and red-shifted spectral lobes. Based on an Yb-fiber ultrafast laser at 1030 nm, we obtained ~100-fs (nearly transform-limited) pulses, tunable from 825 nm to 1210 nm with >1-nJ pulse energy. By using LMA fibers for spectral broadening, we further increased the pulse energy up to 20 nJ in the wavelength range of 1030-1215 nm [22]; such a powerful source enabled us to drive a video-rate laser scanning microscope to study human skin based on harmonic imaging [22]. In this paper, we apply this method to an Er-fiber laser and demonstrate a femtosecond source tunable from 1300 to 1700 nm. Femtosecond pulses tunable in this wavelength range are of particular importance because they are suitable to drive three-photon microscopy [23] that offers increased penetration depth for tissue imaging [19,20,24]. Results from Xu's group demonstrate that three-photon excitation fluorescence microscopy at 1300-1700 nm can achieve >1-mm penetration depth due to an optimal combination of light scattering and water absorption within the biological tissue at this wavelength range [19,20,24].

In this paper, we demonstrate an Er-fiber laser enabled, energy scalable femtosecond source producing >4.5-nJ pulse energy in the 1300-1700 nm wavelength range. Using fibers with larger mode-area and proper dispersion, >10-nJ pulse energy is achieved and the pulse duration can be as short as ~50 fs.

2. Numerical simulation of fiber-optic spectral broadening

Before we present the experimental results, we first use numerical simulations to illustrate our method of implementing wavelength tunable femtosecond sources. The essence of this method is to minimize the dispersion effect during the fiber-optic spectral broadening. Consequently SPM-dominated spectral broadening dramatically expands the input spectrum, forming a series of well separated spectral lobes. The leftmost and rightmost spectral lobes are usually much stronger than other lobes. Use of proper optical bandpass filters to select the leftmost/rightmost spectral lobe produces nearly transform-limited femtosecond pulses.

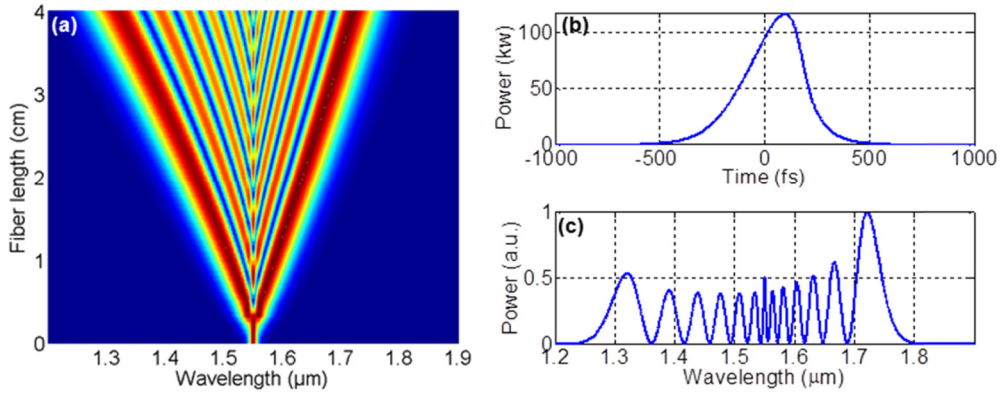

Fig. 1. Simulation results of a 300-fs pulse with 40-nJ pulse energy propagating in an optical fiber with zero GVD. (a) spectral evolution along fiber length. The pulse and the spectrum after 4-cm propagation are plotted in (b) and (c).

We solve the generalized nonlinear Schrödinger equation to simulate the propagation of a 40-nJ, 300-fs hyperbolic-secant pulse (wavelength centered at 1.55 μm) in an optical fiber with the fiber dispersion neglected. The fiber has a mode-field diameter (MFD) of 4 μm. Figure 1(a) shows the optical spectral evolution along the fiber length. As expected, the optical spectrum is dramatically broadened towards both shorter and longer wavelength, manifesting as isolated spectral lobes. The pulse and the spectrum after 4-cm propagation are plotted in Figs. 1(b) and 1(c). Due to the absence of dispersion, the pulse duration changes slightly while self-steepening leads to an asymmetric pulse with the trailing edge sharper than the leading edge.

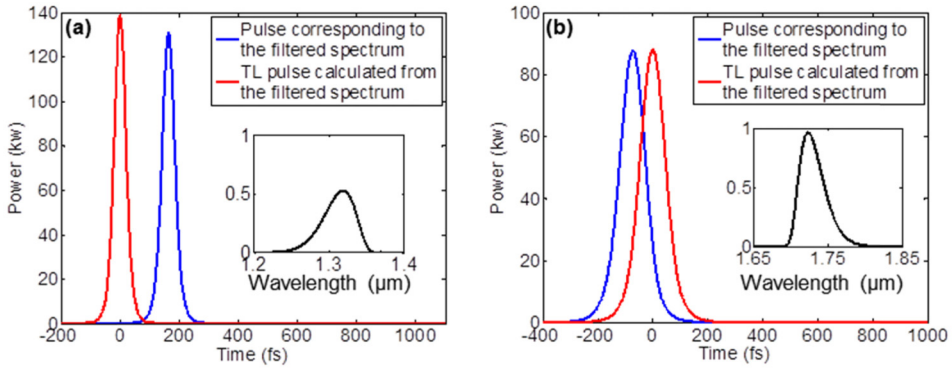

Fig. 2. Corresponding optical pulses (blue curve) and the calculated TL pulses (red curve) from the filtered spectra are shown in (a) for the leftmost lobe and in (b) for the rightmost lobe. Insets: filtered optical spectra. TL: transform-limited.

Figure 1(c) shows that the broadened spectrum comprises 13 isolated spectral lobes with the leftmost one peaking at 1319 nm and the rightmost one at 1724 nm. We then numerically filter both the leftmost and the rightmost spectral lobes, and plot them as the insets of Figs. 2(a) and 2(b). The blue curves in these two figures are the corresponding pulses due to spectral lobe filtering and the red curves are the transform-limited pulses calculated from the leftmost/rightmost spectral lobes (i.e., the spectral shown as the black curves in the insets of Fig. 2). More specific, the filtered leftmost spectral lobe produces 51-fs, 6.6-nJ pulses and the rightmost spectral lobe produces 109-fs, 9.6-nJ pulses. The transform-limited pulses calculated from the filtered spectra are 48 fs and 108 fs in duration, respectively, showing that the filtered pulses are nearly transform-limited.

To illustrate the effect of the GVD (denoted by β_2) and the third-order dispersion (TOD, denoted by β_3), we redo the simulation for three different dispersion combinations: ($\beta_2 = 40$ fs^2/mm, $\beta_3 = 0$), ($\beta_2 = 40$ fs^2/mm, $\beta_3 = 200$ fs^3/mm), and ($\beta_2 = 40$ fs^2/mm, $\beta_3 = -200$ fs^3/mm). We keep all other parameters unchanged and plot the broadened spectra in Fig. 3. The blue curve shows the broadened spectrum using the fiber with constant GVD of 40 fs^2/mm ($\beta_3 = 0$). Comparison of this curve and the blue curve in Fig. 1(c) indicates that positive GVD has two consequences: (1) the broadened spectrum becomes narrower and (2) the spectral-lobe structures tend to wash out manifesting as shallower spectral valleys. TOD leads to frequency-dependent GVD and plays an important role as well. For a positive TOD ($\beta_2 = 40$ fs^2/mm, $\beta_3 = 200$ fs^3/mm), GVD decreases with an increased wavelength and the resulting optical spectrum is broadened more towards longer wavelength (red dotted curve in Fig. 3). Compared with the constant GVD case (blue curve in Fig. 3), positive TOD generates deeper (shallower) spectral valleys on the long (short) wavelength side. In contrast, negative TOD ($\beta_2 = 40$ fs^2/mm, $\beta_3 = -200$ fs^3/mm) causes the spectrum broadened more towards shorter wavelength, with the shallower (deeper) spectral valleys on the long (short)

wavelength side. The simulation results in Fig. 3 suggest that fiber-optic spectral broadening and formation of clear spectral lobes benefit from a smaller positive GVD.

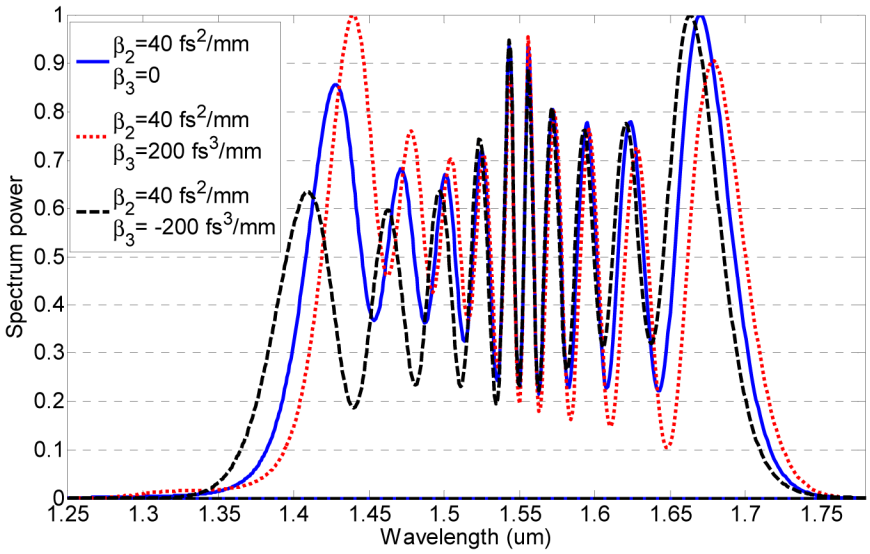

Fig. 3. Simulation results of a 300-fs pulse with 40-nJ pulse energy propagating in 4-cm optical fiber (MFD of 4 μm) with different dispersion combinations: ($\beta_2 = 40$ fs^2/mm, $\beta_3 = 0$), ($\beta_2 = 40$ fs^2/mm, $\beta_3 = 200$ fs^3/mm), and ($\beta_2 = 40$ fs^2/mm, $\beta_3 = -200$ fs^3/mm). β_2 and β_3 denote the GVD and the TOD.

Indeed the detrimental effect caused by dispersion can be reduced by using shorter fibers since dispersion is distributed along the fiber. To maintain spectral broadening, a shorter fiber demands higher input pulse energy to accumulate enough nonlinear phase during pulse propagation. Figure 4 shows the broadened spectra for three combinations of input pulse energy (E) and fiber length (L): ($E = 40$ nJ, $L = 4$ cm), ($E = 80$ nJ, $L = 2$ cm), and ($E = 160$ nJ, $L = 1$ cm). The fiber has a constant GVD of 40 fs^2/mm ($\beta_3 = 0$) and a MFD of 4 μm, and the input hyperbolic-secant pulse has a duration of 300-fs. Although the product of input pulse energy and fiber length is fixed at 160 nJ·cm, shorter fiber and higher pulse energy produces more spectral broadening with deeper spectral valleys due to less dispersion effect; more important, the resulting leftmost and rightmost spectral lobes account for more pulse energy. For example, the leftmost and rightmost spectral lobes peak at 1.37 μm and 1.70 μm for 1-cm fiber with 160-nJ input pulse energy (red dotted curve in Fig. 4). Filtering these two spectral lobes generates ~100-fs, nearly transform-limited pulses with 32-nJ (40-nJ) pulse for the leftmost (rightmost) spectral lobe. Clearly using shorter fiber and higher input pulse energy for spectral broadening constitutes an efficient and energy scalable means to obtain high-energy, wavelength widely tunable femtosecond pulses.

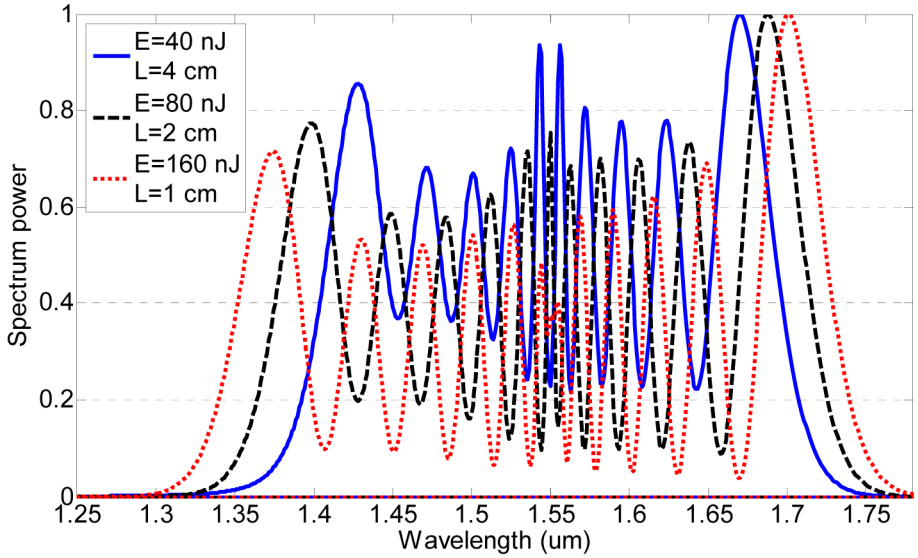

Fig. 4. Simulation results of a 300-fs hyperbolic-secant pulse propagating in an optical fiber (MFD of 4 μm) with different combination of input pulse energy (E) and fiber length (L). The fiber has a positive GVD of 40 fs^2/mm.

3. Experimental results

Guided by the simulation results in the previous section, we constructed such an energy scalable femtosecond source tunable from 1.3 to 1.7 μm based on a high-power Er-fiber laser system schematically shown in Fig. 5.

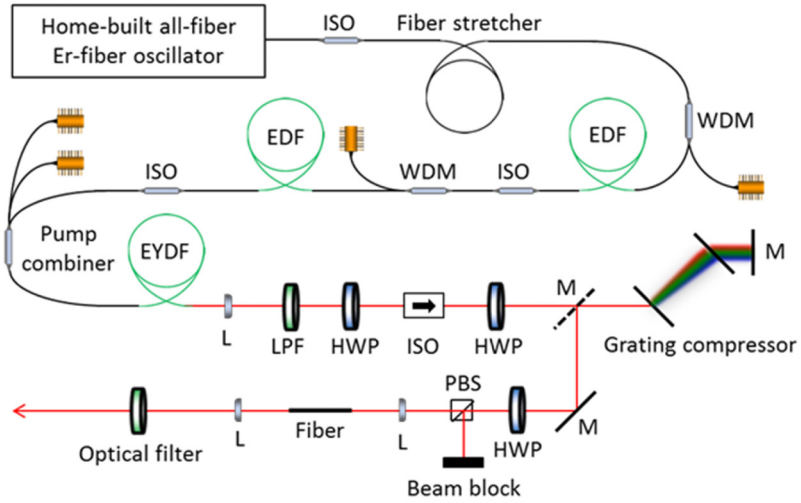

Fig. 5. Experimental setup. WDM: wavelength-division multiplexing, EDF: erbium-doped fiber, EYDF: erbium ytterbium co-doped fiber, L: lens, M: mirror, ISO: isolator, HWP: half-wave plate, PBS: polarization beam splitter, LPF: long pass filter.

The Er-fiber laser system used a master-oscillator-power-amplifier architecture, in which the oscillator pulses were amplified using the well-known chirped-pulse amplification (CPA) technique. The home-built 31-MHz Er-fiber oscillator was configured in a ring structure mode-locked by a semiconductor saturable absorber (from Batop), producing ~100-pJ pulses centered at 1550 nm [25]. We intentionally set the repetition rate at 31 MHz in order to enable

video rate (i.e., 30 frames per second) image recording in a laser-scanning microscope, assuming that each image consists of 512 × 512 pixels with 4 pulses per pixel. A fiber stretcher with positive GVD stretched the oscillator pulses to ~15 ps, which were then amplified to 8-nJ pulse energy by two stages of pre-amplification. The main amplifier was constructed using an Er:Yb co-doped fiber (polarization-maintaining fiber with 17 μm core diameter) pumped by two laser diodes. The amplified 200-nJ pulses were dechirped by a diffraction-grating (966.2 lines/mm groove density) pair configured at double-pass with 80% transmission efficiency.

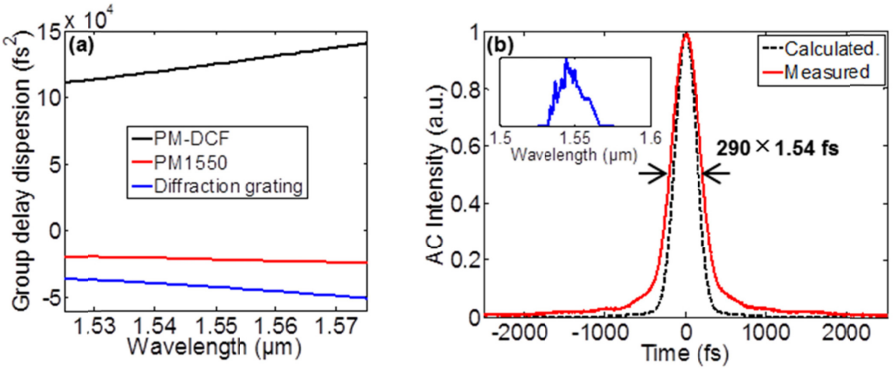

Fig. 6. (a) GDD contribution of 1-m PM DCF, 1-m PM1550, and 1-mm diffraction-grating pair. (b) Measured autocorrelation trace (red) of the compressed pulse and calculated autocorrelation trace (black dashed) of the transform-limited pulse allowed by the optical spectrum. Inset: Optical spectrum of the compressed pulse. It is plotted in linear scale.

To generate high-quality pulses, the total dispersion (especially the third-order dispersion, TOD) of the CPA system must be carefully managed. The grating-pair provided negative group-delay dispersion (GDD) and positive TOD (blue curve in Fig. 6(a)), which requires a fiber stretcher with positive GDD and negative TOD. Our fiber stretcher consisted of polarization-maintaining (PM) dispersion-compensating fiber (DCF) and conventional SMF PM1550. The PM DCF provides positive GDD and negative TOD (black curve in Fig. 6(a)), while PM1550 exhibits negative GDD and positive TOD (red curve in Fig. 6(a)). An optimal length combination of these two fibers allowed fine tuning of total dispersion. Figure 6(b) shows the measured autocorrelation trace (red curve) of the compressed pulse. The pulse duration is estimated to be 290 fs assuming a hyperbolic secant pulse profile. Inset of Fig. 6(b) records the optical spectrum of the compressed pulse. Black dashed curve in Fig. 6(b) indicates the calculated autocorrelation trace of the transform-limited pulse allowed by the optical spectrum. Apparently the compressed pulse is close to be transform-limited.

Table 1. Properties of optical fibers used for spectrum broadening

Type	λ_{ZDW} nm	D@1550 nm ps/(nm*km)	β_2@1550 nm fs^2/mm	β_3@1550 nm fs^3/mm	MFD@1550 nm μm	γ@1550 nm $W^{-1}km^{-1}$
HNLF	1518	0.32	–0.408	10.4	4	10.8
DCF3	1610	–3	3.83	75	8	2.7
DCF38	1250	–38.5	48.5	–284	6	4.8

The compressed pulse with 160-nJ pulse energy was coupled into an optical fiber for nonlinear spectral broadening followed by a proper optical filter to select the leftmost/rightmost spectral lobe. A half-wave plate and a polarization beam splitter were used to adjust the pulse energy coupled into the fiber. We tested three commercially available optical fibers: highly nonlinear fiber (HNLF, from OFS), DCF3 (from Thorlabs), and DCF38 (from Thorlabs). Their optical parameters are listed in Table 1.

HNLF features low dispersion in the wavelength range of 1.3-1.7 μm, well suited for implementing SPM-dominated spectral broadening. The blue curves in Fig. 7 represent the output spectra from 4-cm HNLF at different input pulse energy of 11 nJ, 16 nJ, 22 nJ, 26 nJ, and 30 nJ. Clearly, the spectrum broadens with increasing pulse energy and forms well-isolated spectral lobes indicating that the spectral broadening is dominated by SPM. With 30-nJ pulse energy coupled into the HNLF, the leftmost spectral lobe peaks at 1.3 μm and the rightmost one at 1.7 μm. To investigate the energy scaling property offered by shortening the fiber length, we prepared another 2-cm long HNLF and adjusted the coupled pulse energy such that the resulting rightmost spectral lobes peak at the same wavelength as those obtained from the 4-cm HNLF. Red dashed curves in Fig. 7 record these output spectra with the coupled pulse energy labeled for each curve. To have a better comparison, we normalize the curves for an optimized overlapping. Since shortening the fiber length reduces the accumulated dispersion effect—as demonstrated by simulation results in Fig. 4, the ratio of pulse energies coupled into the 2-cm and 4-cm HNLF is slightly less than two to achieve the same amount of spectral broadening.

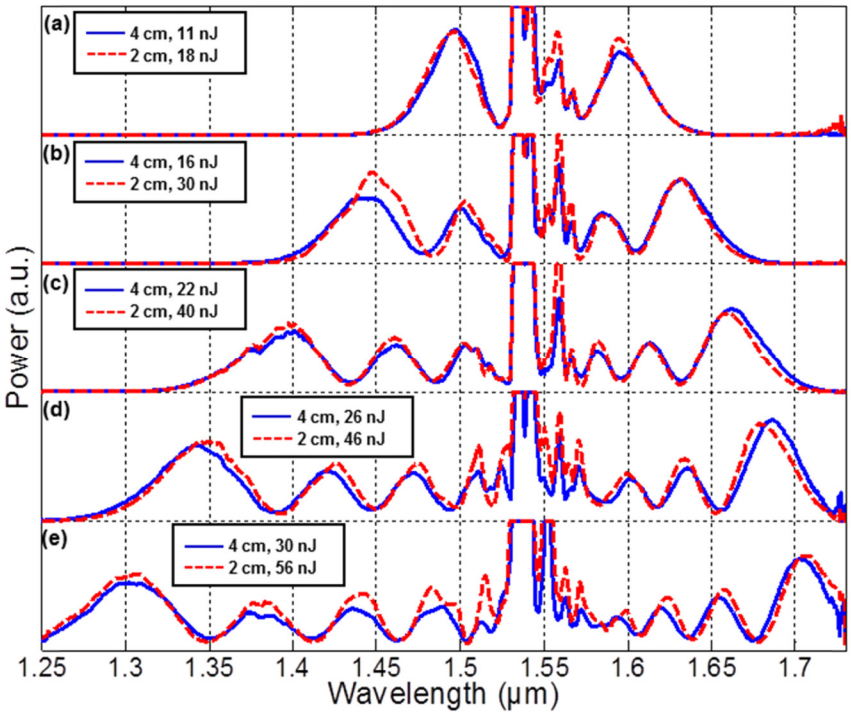

Fig. 7. Output spectra from HNLF at different fiber length (4 cm versus 2 cm) and pulse energy. We adjust the input pulse energy such that the spectra generated by both fibers have their rightmost spectral lobes peaking at (a) 1.59 μm, (b) 1.63 μm, (c) 1.66 μm, (d) 1.68 μm, and (e) 1.71 μm. Coupled pulse energies for each fiber are presented in each figure as well.

To obtain wavelength tunable femtosecond pulses, we varied the coupled pulse energy into the 2-cm HNLF and then used a set of optical filters (bandpass, ~50 nm bandwidth) to select the leftmost or the rightmost spectral lobes; Fig. 8 presents six representative filtered spectral lobes (Left column). They peak at 1.3 μm, 1.35 μm, 1.4 μm, 1.45 μm, 1.6 μm, and 1.7 μm with the corresponding pulse energy of 4.5 nJ, 4.8 nJ, 4.9 nJ, 5.2 nJ, 5.2 nJ, and 7.1 nJ, respectively. In contrast, the pulse energies at these six wavelengths using 4-cm HNLF are 2.3 nJ, 2.3 nJ, 2.7 nJ, 2.9 nJ, 2.9 nJ, and 3.4 nJ, respectively. As expected, they are about one half of the pulse energies given by the 2-cm HNLF. At a repetition-rate of 31 MHz, this tunable femtosecond source enabled by the 2-cm HNLF has the average power between 140

and 220 mW. The corresponding pulses were measured by an intensity autocorrelator and the measured autocorrelation traces are shown as the red curves in the right column of Fig. 8. The FWHM duration of these autocorrelation traces is in the range of 149-280 fs. The pulse duration is estimated to be 97-182 fs, assuming a hyperbolic-secant pulse with a deconvolution factor of 1.54. The black dashed curves in the right column plot the calculated autocorrelation traces of the transform-limited pulses allowed by the filtered spectra, showing that the filtered spectra correspond to nearly transform-limited pulses.

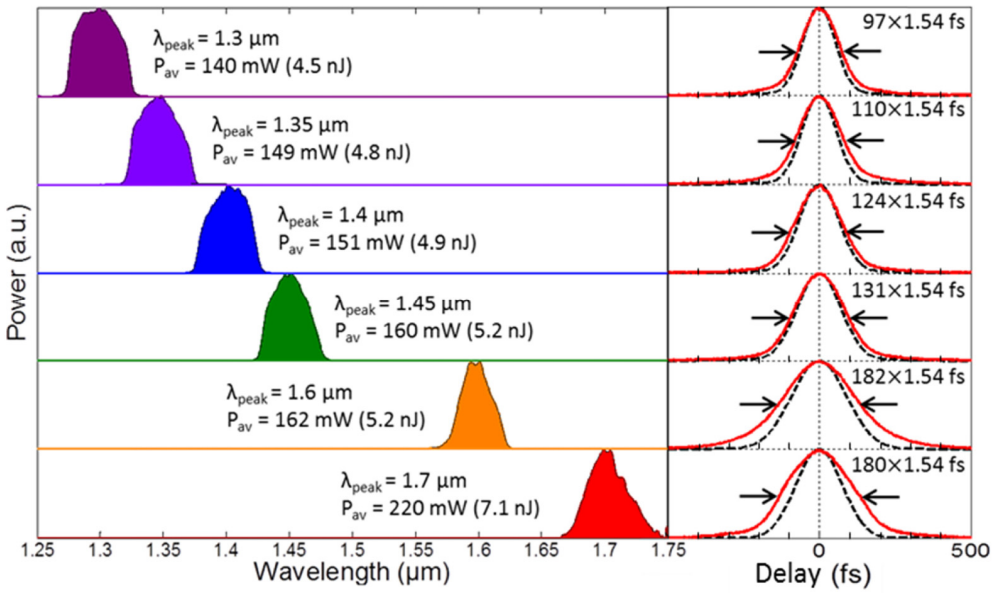

Fig. 8. (Left column) Filtered optical spectra from 2-cm HNLF; their peak wavelength, average power, and pulse energy are labeled in the figure. (Right column) Measured autocorrelation traces (red solid curves) and autocorrelation traces calculated from the transform-limited pulses allowed by the filtered spectra (black dotted curves).

Besides energy scaling by shortening the optical fiber, using fibers with larger MFD is another option. In addition, larger MFD makes the free-space power coupling into the fibers less environmentally sensitive. Fiber DCF3 and DCF38 exhibit positive GVD at 1.55 μm with their MFD (8 μm for DCF3 and 6 μm for DCF38) larger than the HNLF. Interestingly DCF3 has a positive TOD (75 fs^3/mm) and DCF38 a negative TOD (–284 fs^3/mm). Figure 9 shows the spectral broadening from these two fibers, both of which are 4-cm in length. To have a fair comparison, we couple 42-nJ pulse energy into DCF3 and 31-nJ pulse energy into DCF38 such that the rightmost spectral lobes generated by both fibers peak at 1.625 μm. As we expect from simulation results in Fig. 4, negative TOD allows DCF38 to shift the leftmost spectral lobe at a wavelength shorter than that obtained from fiber DCF3 with positive TOD. Apparently fiber DCF38 exhibits broader wavelength tuning range than can be achieved by fiber DCF3 at the same input pulse energy.

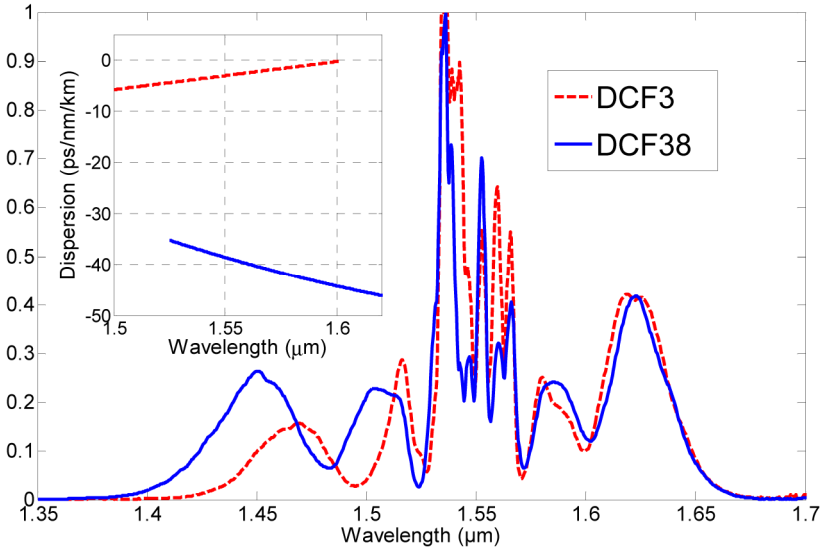

Fig. 9. Output spectra from DCF3 and DCF38. Both of them are 4-cm long. Inset: dispersion of DCF3 and DCF38.

With the input pulse energy at 96 nJ, 63 nJ, 21 nJ, and 96 nJ, 4-cm DCF38 allows us to produce four filtered spectral lobes peaking at 1.35 μm, 1.4 μm, 1.6 μm, and 1.7 μm (Left column of Fig. 10). Note that these four spectra are filtered by either low-pass (spectra peaking at 1.35 μm and 1.4 μm) or long-pass optical filters (spectra peaking at 1.6 μm and 1.7 μm) to obtain broader spectra than can be achieved by optical bandpass filters. As a result, the filtered spectra exhibit larger spectral bandwidth than those shown in Fig. 8. The corresponding pulses have the energy of 10.3 nJ, 8.8 nJ, 7.4 nJ, and 10.6 nJ, respectively. The red curves in the right column of Fig. 10 plot the measured autocorrelation traces. Compared with the calculated autocorrelation traces of the transform-limited pulses (black dashed curves), the resulting pulses deviate considerably from transform-limited pulses mainly caused by the large GVD of fiber DCF38. Since both positive GVD and SPM exert positive chirp to the propagating pulse, bulk materials with negative GVD can be used to dechirp the pulses given by the filtered spectra. We employ several fused-silica plates to dechirp these pulses. The measured autocorrelation traces of the dechirped pulses are shown as the purple curves in the right column of Fig. 10. They nearly overlap with the black dashed curves showing that the dechirped pulses are nearly transform-limited. The pulse duration is estimated to be 52-143 fs, assuming a hyperbolic-secant pulse with a deconvolution factor of 1.54.

Apparently SPM-dominated spectral broadening in DCF38 produced femtosecond pulses with higher pulse energy and shorter pulse duration than using HNLF. For example, the 1.35-μm pulses generated by 4-cm DCF38 possess 10.3-nJ energy and 53-fs duration while 2-cm HNLF produces the 1.35-μm pulses with 4.8-nJ energy and 110-fs duration. This means that the pulse peak power differs by a factor of 4 for these two 1.35-μm sources. Use of a femtosecond source with higher pulse energy and shorter pulse duration is of particular importance to increase the signal strength in multiphoton microscopy. For three-photon microscopy, the signal becomes 32 times stronger if the driving pulse duration is reduced by a factor of 2 while the pulse energy is doubled [26].

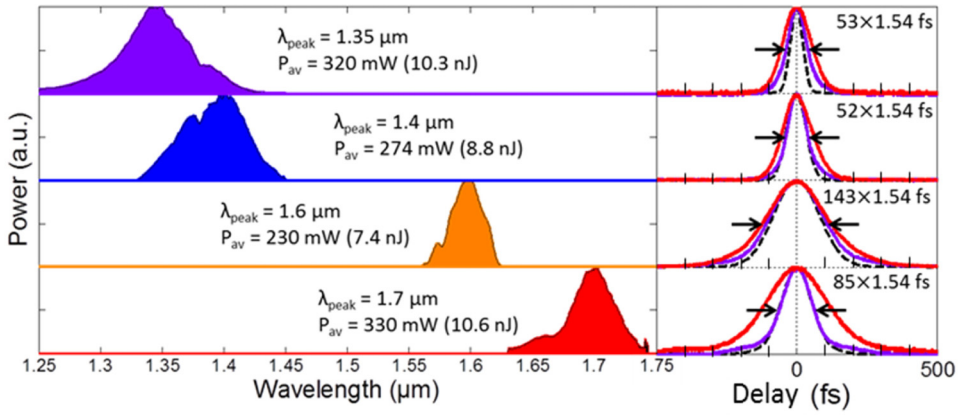

Fig. 10. (Left column) Filtered optical spectra from 4-cm DCF38. Their peak wavelength, pulse energy, and average power are labeled in the figure. (Right column) Measured autocorrelation traces of the pulses before (red curves) and after (purple curves) being dechirped by fused silica plates. Black dashed curves plot the calculated autocorrelation traces of the transform-limited pulses allowed by the filtered spectra.

4. Conclusion and discussion

We present a detailed numerical and experimental study of SPM-dominated spectral broadening of narrowband spectra generated by an Er-fiber laser system. Using proper optical filters to select the leftmost or rightmost spectral lobes results in ultrafast sources widely tunable from 1.3 to 1.7 μm with the pulse energy up to >10-nJ and the pulse duration as short as ~50 fs. Currently we are applying this tunable source to deep tissue three-photon microscopy.

Compared with SSFS-enabled ultrafast source, our laser source features broader wavelength coverage and superior energy scalability. The ultimate limit of our method is the fiber damage caused by self-focusing when the input pulse peak power exceeds 9 MW—the self-focusing threshold for fused silica fibers at 1.55 μm. This power level can be reached when the input 300-fs pulse has an energy of ~2.7 μJ. With 10-20% conversion efficiency depending on the amount of wavelength shift, >200-nJ femtosecond pulses tunable from 1.3 to 1.7 μm are expected. We plan to upgrade our Er-fiber laser system to ~μJ energy level and demonstrate this energy scalability using fiber DCF3, which has a larger MFD than both HNLF and DCF38. We expect that ~5-mm long DCF3 pumped by ~μJ pulses at 1.55 μm will produce ~100-nJ level pulses tunable from 1.3 to 1.7 μm.

One might think that a fiber of several milli-meter long can be replaced by a free-space bulk material (such as a fused-silica plate) to achieve SPM-enabled spectral broadening. In fact, for the input peak power below self-focusing threshold (9 MW for fused silica at 1.55 μm), diffraction in the bulk material due to lack of waveguide structure rapidly diverges a tightly focused beam causing a negligible nonlinear phase ($<\pi$). To observe significant spectral broadening, the input peak power needs to exceed self-focusing threshold, which triggers other nonlinear processes (e.g., plasma formation) that destroy the spectral-lobe structure featured by SPM-dominated spectral broadening.

In our current experimental setup, the amplified pulses are compressed by a pair of diffraction-gratings. Such a free-space compressor can be replaced by a hollow-core photonic bandgap fiber that is spliced with one end to the amplifier fiber and the output end to the short SPM-broadening fiber. The resulting all-fiber configuration of such an SPM-enabled tunable femtosecond source will be even more robust, compact, and advantageous than the OPO solution.

Funding

Helmholtz Association through the Helmholtz Young Investigator Group (VH-NG-804); Helmholtz-CAS Joint Research Group grant (HCJRG 201).

Acknowledgments

The authors acknowledge financial support by the excellence cluster “The Hamburg Centre for Ultrafast Imaging - Structure, Dynamics and Control of Matter at the Atomic scale” of the Deutsche Forschungsgemeinschaft.